Science Arts & Métiers (SAM)

is an open access repository that collects the work of Arts et Métiers Institute of Technology researchers and makes it freely available over the web where possible.

Prediction of Hip Failure Load: In Vitro Study of 80 Femurs Using Three Imaging Methods and Finite Element Models—The European Fracture Study (EFFECT)[1]

Pierre Pottecher, MD
Klaus Engelke, PhD
Laure Duchemin, PhD
Oleg Museyko, PhD
Thomas Moser, MD
David Mitton, PhD
Eric Vicaut, MD, PhD
Judith Adams, MD
Wafa Skalli, PhD
Jean Denis Laredo, MD
Valérie Bousson, MD, PhD

[1] From the Laboratoire de Radiologie Expérimentale, CNRS UMR 7052, UFR Lariboisière-Saint-Louis, 2 rue Ambroise Paré, 75010 Paris, France (P.P., J.D.L., V.B.); Institute of Medical Physics, University of Erlangen, Erlangen, Germany (K.E., O.M.); LBM/Institut de Biomecanique Humaine Georges Charpak, Arts et Métiers ParisTech, Paris, France (L.D., W.S.); Department of Radiology, Hôpital Notre-Dame, Centre Hospitalier de l'Université de Montréal, Montréal, Québec, Canada (T.M.); Laboratoire de Biomécanique et Mécanique des Chocs-Université Lyon 1–IFSTTAR, Lyon, France (D.M.); Unité de Recherché Clinique Saint-Louis Lariboisère Fernand Widal, Paris, France (E.V.); and Department of Clinical Radiology, The Royal Infirmary, Imaging Science and Biomedical Engineering, University of Manchester, Manchester, England (J.A.).

Purpose: To evaluate the performance of three imaging methods (radiography, dual-energy x-ray absorptiometry [DXA], and quantitative computed tomography [CT]) and that of a numerical analysis with finite element modeling (FEM) in the prediction of failure load of the proximal femur and to identify the best densitometric or geometric predictors of hip failure load.

Materials and Methods: Institutional review board approval was obtained. A total of 40 pairs of excised cadaver femurs (mean patient age at time of death, 82 years $\pm$ 12 [standard deviation]) were examined with *(a)* radiography to measure geometric parameters (lengths, angles, and cortical thicknesses), *(b)* DXA (reference standard) to determine areal bone mineral densities (BMDs), and *(c)* quantitative CT with dedicated three-dimensional analysis software to determine volumetric BMDs and geometric parameters (neck axis length, cortical thicknesses, volumes, and moments of inertia), and *(d)* quantitative CT-based FEM to calculate a numerical value of failure load. The 80 femurs were fractured via mechanical testing, with random assignment of one femur from each pair to the single-limb stance configuration (hereafter, *stance configuration*) and assignment of the paired femur to the sideways fall configuration (hereafter, *side configuration*). Descriptive statistics, univariate correlations, and stepwise regression models were obtained for each imaging method and for FEM to enable us to predict failure load in both configurations.

Results: Statistics reported are for stance and side configurations, respectively. For radiography, the strongest correlation with mechanical failure load was obtained by using a geometric parameter combined with a cortical thickness ($r^2 = 0.66$, $P < .001$; $r^2 = 0.65$, $P < .001$). For DXA, the strongest correlation with mechanical failure load was obtained by using total BMD ($r^2 = 0.73$, $P < .001$) and trochanteric BMD ($r^2 = 0.80$, $P < .001$). For quantitative CT, in both configurations, the best model combined volumetric BMD and a moment of inertia ($r^2 = 0.78$, $P < .001$; $r^2 = 0.85$, $P < .001$). FEM explained 87% ($P < .001$) and 83% ($P < .001$) of bone strength, respectively. By combining *(a)* radiography and DXA and *(b)* quantitative CT and DXA, correlations with mechanical failure load increased to 0.82 ($P < .001$) and 0.84 ($P < .001$), respectively, for radiography and DXA and to 0.80 ($P < .001$) and 0.86 ($P < .001$), respectively, for quantitative CT and DXA.

Conclusion: Quantitative CT-based FEM was the best method with which to predict the experimental failure load; however, combining quantitative CT and DXA yielded a performance as good as that attained with FEM. The quantitative CT DXA combination may be easier to use in fracture prediction, provided standardized software is developed. These findings also highlight the major influence on femoral failure load, particularly in the trochanteric region, of a densitometric parameter combined with a geometric parameter.

The incidence of osteoporotic fractures increases exponentially with age in both women and men and is generating a growing societal, economic, and personal burden as the world population ages (1). Osteoporosis is defined as low bone mineral density (BMD) combined with bone microarchitecture alterations, which impair bone strength and therefore increase fracture risk. Proximal femoral fractures are common and are associated with substantial morbidity and mortality (2,3). Bone densitometry with dual-energy x-ray absorptiometry (DXA) is the reference standard in the diagnosis of osteoporosis and monitoring of therapeutic efficacy (4,5). However, in the Rotterdam cohort, among women with nonvertebral osteoporotic fractures, only 44% were classified as having osteoporosis with DXA (6). This finding highlights the need to measure other bone properties, such as bone geometry, to accurately evaluate the fracture risk. Other techniques have proven effective in predicting fractures. First, pelvic radiography yielded a good estimate of bone strength via simple measures, such as the neck shaft angle and cortical thickness (7,8). Quantitative computed tomography (CT) with combined analysis of geometric and densitometric parameters is a powerful tool with which to assess bone strength (9–11). The most recent method is finite element modeling (FEM) based on quantitative CT data sets and involving a combined geometric and mechanical approach. FEM can be used to determine the load that causes bone failure under defined conditions. FEM has been found to be superior to DXA in the prediction of fractures (12). Although FEM recently has been applied in vivo (13,14), it is not used in everyday clinical practice.

In this article, we report the findings of an in vitro study in which we compared the performance of FEM and three imaging methods—namely, radiography, DXA, and quantitative CT—in the prediction of bone strength. Our primary objective was to evaluate the performance of these three imaging methods and that of FEM in the prediction of failure load of the proximal femur. Our secondary objective was to identify the best densitometric or geometric predictors of hip failure load.

Materials and Methods

Institutional review board approval was obtained from the Institute of Anatomy (Paris-Descartes University, Paris, France). Forty pairs of excised femurs were analyzed by using radiography, DXA, quantitative CT, and FEM and were submitted to mechanical testing. The study, part of a European contract (contract number QLK6-CT-2002-02440-3DQCT) was conducted over 10 years. The femurs were collected between November 2003 and March 2004. Radiography and DXA were performed in 2004, radiographic measurements were obtained in 2004, quantitative CT images were acquired in 2005, and mechanical tests were performed in 2005 after quantitative CT. Quantitative CT images were analyzed in 2006 and were reanalyzed in 2012 by using the latest version of dedicated software (MIAF [Medical Image Analysis Framework]-Femur Option, version 6.2.0; Institute of Medical Physics, University of Erlangen, Germany) (15). Finite element models were generated in 2006 and were validated in 2010. Figure 1 shows the different steps of the study.

The same set of femurs studied here was also used to predict the failure load using texture analysis on radiographs (16). A previous in vitro study by our group, focused on predicting the failure load with quantitative CT, used a smaller set of femurs different from those used in this study (10).

Femurs

We studied 40 pairs of femurs obtained at the Institute of Anatomy (Paris-Descartes University, Paris, France) from 24 women and 16 men aged 47–100 years at the time of death (mean age, 82 years ± 12 [standard deviation]) who had donated their bodies to science. The femurs were harvested in compliance with institutional safety regulations and were kept at −20°C after soft-tissue removal. The diaphysis of each femur was sliced 10 cm below the lesser trochanter to facilitate bone

Advances in Knowledge

- Geometric and densitometric parameters should be used together to optimize bone failure prediction.
- With the combination of dual-energy x-ray absorptiometry and quantitative CT, we obtained r^2 values of 0.80 and 0.86 for cervical and trochanteric fractures, respectively.
- The trochanteric region deserves careful consideration when predicting bone failure.

Implication for Patient Care

- The findings of our in vitro study should help us improve the identification of populations at risk for osteoporotic hip fractures and obtain accurate risk predictions with several simple or sophisticated methods.

fixation for quantitative CT and mechanical testing. No information was available on mobility before death.

Radiography

Anteroposterior radiographs of each femur were obtained with the femur placed on a Prestige table (GE Medical Systems, Milwaukee, Wis). The femur was positioned in medial rotation, with a wedge placed under the lateral condyle to correct femoral neck anteversion relative to the shaft, thereby bringing the neck parallel to the table. The femoral head, greater trochanter, and medial condyle were in contact with the table. The femur was placed directly on a 35 × 43 cm cassette containing medium-sensitivity film (Kodak, Paris, France). Exposure parameters were the same for all femurs (120-cm focus-to-film distance, 45 kV, 4 mAs).

Two radiologists (V.B., T.M., 6 years and 1 year of experience, respectively, in musculoskeletal radiology at the time of measurement) independently measured radiography variables potentially involved in bone strength (8,17). The readers were blinded to all information about the cases (age of the subjects and results of DXA, quantitative CT, FEM, and mechanical testing). Measurements were obtained by using a plastic ruler marked at 0.5-mm intervals placed directly on the film hard copies. Before starting the measurement sessions, the readers worked together to check the position of the points on randomly selected femurs. The mean of the two independent measurements for each geometric parameter was used for statistical analyses. Interreader reproducibility was assessed by using pairs of values from 10 femurs taken at random. Intrareader reproducibility was evaluated by having the junior reader perform a second set of measurements 3 weeks after the first reading in 10 femurs chosen at random. Coefficients of variation were calculated according to the method described by Glüer et al (8).

Sixteen geometric parameters were measured (Fig 2). Six parameters were cortical thicknesses: *(a)* inferior cortical femoral neck thickness, *(b)* superior cortical femoral neck thickness,
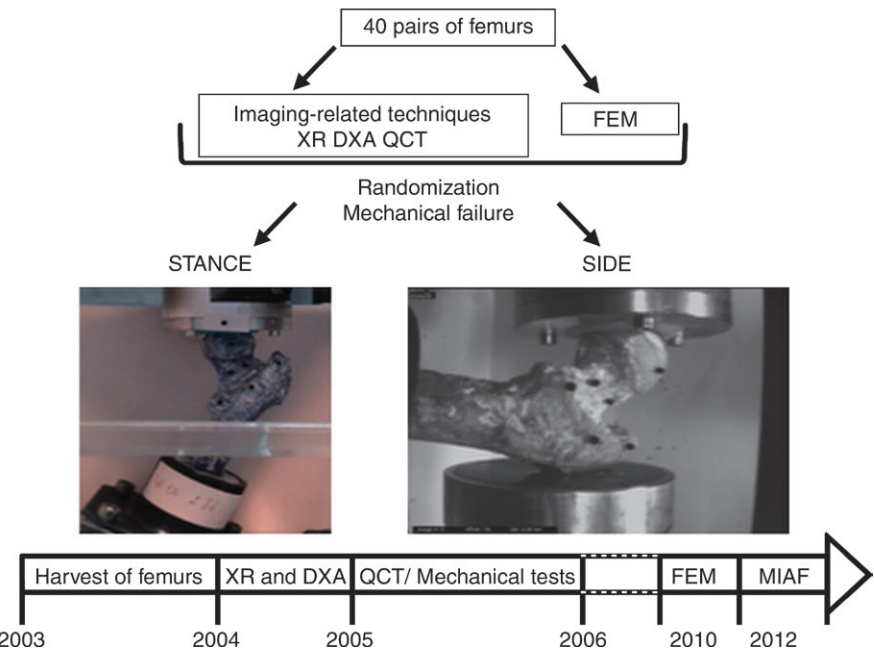
Figure 1: Flowchart shows the different steps of the study. *QCT* = quantitative CT, *XR* = radiography.
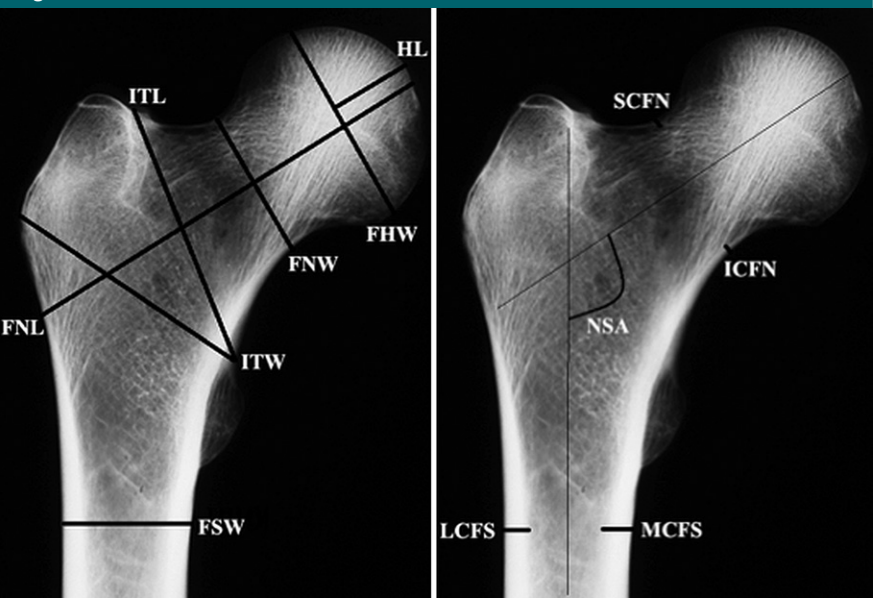
Figure 2: Hip radiographs show the 16 geometric parameters measured manually. Left: *FHW* = femoral head width, *FNL* = femoral neck length, *FNW* = femoral neck width, *FSW* = femoral shaft width, *HL* = head length, *ITL* = intertrochanteric length. Right: *ICFN* = inferior cortical femoral neck thickness, *LCFS* = lateral cortical femoral shaft thickness, *MCFS* = medial cortical femoral shaft thickness, *NSA* = neck shaft angle, *SCFN* = superior cortical femoral neck thickness.

(c) medial cortical femoral shaft thickness, *(d)* lateral cortical femoral shaft thickness, *(e)* medial cortical middiaphyseal thickness, and *(f)* lateral cortical middiaphyseal thickness. The remaining 10 parameters were distances: *(a)* femoral neck length, *(b)* femoral head width, *(c)* femoral neck width, *(d)* femoral shaft width, *(e)* middiaphyseal width, *(f)* intertrochanteric height, *(g)* intertrochanteric length, *(h)* head length, *(i)* intertrochanteric width (ITW), and *(j)* neck shaft angle.

DXA Technique

Each femur was immersed in a water bath to simulate soft tissue and was examined with DXA (Delphi W; Hologic, Bedford, Mass). Areal BMD (in grams per square centimeter) was measured at the femoral neck, greater trochanter, and total hip.

Quantitative CT Technique

Image acquisition.—A four-row CT scanner (Somatom Volume Zoom 4; Siemens, Erlangen, Germany) was used. The diaphysis was fixed in a specifically designed system that positioned the femur in medial rotation. The femur was immersed in a water-filled tank, as water simulates soft-tissue x-ray absorption. A solid calibration phantom (Osteo Phantom; Siemens, Munich, Germany) was placed under the tank and scanned simultaneously with each femur to convert attenuation (in Hounsfield units) into bone-equivalent units (in milligrams per milliliter hydroxyapatite). The phantom consisted of a water-equivalent component (0 mg/mL) and a bone-equivalent component (200 mg/mL hydroxyapatite). Scanning extended from the top of the femoral head to 5 cm below the lesser trochanter. CT scanning was performed with 4×1 mm detector collimation (ie, four detectors with 1-mm section thickness), 120 kV, 100 mAs, and 0.75 pitch. From the raw data, 1.00-mm-thick transverse images were reconstructed with a 0.7-mm increment, 150-mm field of view, 250-μm in-plane pixel size (matrix, 512×512 pixels), and B40 kernel.
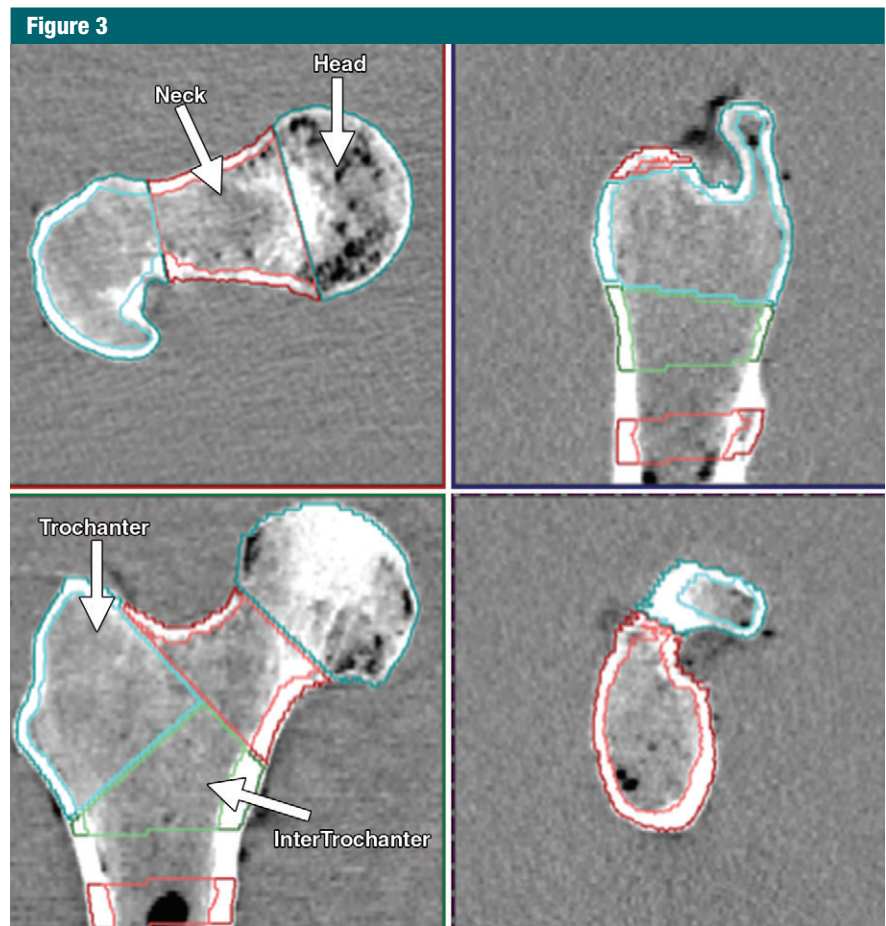

Figure 3: Interface of the dedicated image analysis software.

Image analysis.—Quantitative CT images were analyzed by using the aforementioned dedicated femur software (15) (Fig 3). Five volumes of interest (VOIs) were automatically defined in three dimensions from the automatic determination of a neck coordinate system established with MIAF software: femoral head, femoral neck, NeckBOX, trochanter, and intertrochanter. In addition, one planar section through the trochanter (TrochanterSection) was included in the analysis (Fig 4). Three bone compartments were defined: trabecular, cortical, and integral. For each VOI compartment, we measured bone mineral content (BMC, in milligrams), volume (in milliliters), and BMD (in milligrams per milliliter).

The geometric parameters were hip axis length and cortical thickness in all VOIs except the head. In addition, axial and polar moments of inertia, as well as axial and polar cross-sectional moments of inertia, were determined with NeckBOX and TrochanterSection.

FEM Technique

For each femur, a femur-specific FEM was generated, as described by Duchemin et al (18). The subject-specific mesh was obtained by using deformation of a parameterized generic hexahedral mesh, which approximately replicated the generic femoral anatomy. For each femur, this generic mesh was registered in the CT scan coordinate system, and homothetic transformation was used to scale the mesh to the CT data of the individual specimen. Then, an iterative process of nonlinear deformation and smoothing was applied to personalize the periosteal surface represented by
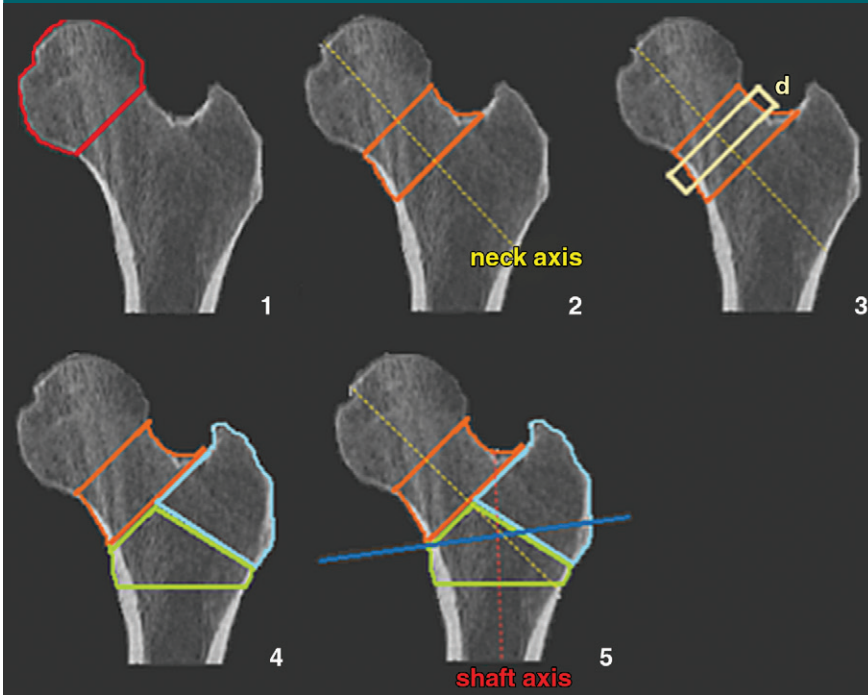
Figure 4: Representation of the VOIs determined with the aforementioned imaging software. The different VOIs are, *1*, the femoral head (red), *2*, the femoral neck (orange), *3*, NeckBox (yellow box), *4*, the trochanter (blue) and the intertrochanter (green) and, *5*, the TrochanterSection (blue line).

the external nodes of the mesh and the cortical bone thickness using the second node layer of the mesh. Mesh quality was evaluated by analyzing element distortion. Residual distortions were corrected automatically. The Young modulus and ultimate stress of each element were calculated from its BMD value by using relationships obtained for cortical and cancellous bone (18).

The boundary conditions applied to the FEM replicated mechanical testing in the single-limb stance or sideways-fall configuration. The numerical failure load was considered to be reached once 50 contiguous elements in the cortical bone had exceeded their ultimate stress. Ansys software (Ansys, version 11.1; ANSYS, Cecil Township, Pa) was used for numerical analyses.

Mechanical Testing

Mechanical testing was performed in both the single-limb stance configuration (hereafter, *stance configuration*) and the sideways fall configuration (hereafter, *side configuration*). The ability of each modality to be used to predict the failure load was determined for each configuration. Within each of the 40 pairs, the femurs were randomly assigned to either the stance configuration or the side configuration to simulate the mechanisms of cervical and trochanteric fractures, respectively. A universal testing machine (5500 Series; Instron, Norwood, Mass) was used to perform tests designed to fracture the proximal femur (19). For the stance configuration, the diaphysis, cut 10 cm below the lesser trochanter, was embedded in a low-melting-point alloy and fixed so that the diaphyseal axis was inclined 25° relative to the vertical line in the coronal plane. The force was applied vertically to the femoral head at a speed of 12.7 mm/min (Fig 1). For the side configuration, the femoral shaft was set at a 10° angle from the horizontal plane, with 15° of internal rotation. The greater trochanter was loaded by using a rubber cup (Fig 1). In both configurations, the femoral head was molded with

polymethylmethacrylate to ensure force distribution over an appropriate surface area. The experimental failure load (in newtons) was determined at the maximal recorded load.

Statistical Analyses

Statistical analyses were performed separately for stance and side configurations. For each variable, we computed the mean, standard deviation, and range. We then performed univariate analysis to compute the Pearson coefficient *(r)* for associations linking the independent variables obtained by using radiography, DXA, quantitative CT, and FEM to the experimental failure load (dependent variable). For multivariate analysis, to detect and avoid overfitting and multicollinearity due to the large number of variables relative to the small number of femurs, we used the random forest approach (20) to identify the most significant variables. Then, we built a stepwise regression model with backward selection (*P* cutoffs of .10 for entry and .20 for removal) using a robust variance estimator. Fractional polynomials were used to find the best-fitting form of continuous predictors. For each model, we obtained the coefficient of the variable, its 95% confidence interval, the adjusted coefficient of determination (r^2), and an estimation of model quality based on the Akaike information criterion (AIC) (21). Finally, we evaluated whether combining *(a)* radiography and DXA or *(b)* DXA and quantitative CT with the method described previously performed better than variables from one modality in predicting the experimental failure load. Statistical tests were performed using statistical software (Stata, version 12; Stata, College Station, Tex). $P < .05$ indicated a significant difference.

Results

Intra- and Interreader Reproducibility of Radiographic Measurements

The mean intrareader coefficient of variation was 4.22% (range, 0%–25.53%), and the mean interreader coefficient of variation was 4.42% (range,

Table 1

Experimental Failure Load

Mechanical Testing	Stance ($n = 40$)	Side ($n = 37$)
Failure load (N)	9031 ± 3444 (3994–15886)	2480 ± 1212 (890–4493)

Note.—Descriptive statistics of experimental failure load obtained with mechanical testing in the two configurations. Data are mean ± standard deviation, with the range in parentheses.

0.68%–25.98%). The thickness of the superior cortical femoral neck was the least reproducible parameter (highest intra- and interreader coefficients of variation).

Descriptive Statistics and Analyses

Descriptive statistics and results of uni- and multivariate regression analyses are reported for 40 femurs in the stance configuration and for 37 femurs in the side configuration. Technical failures occurred during testing of the remaining three femurs. Table 1 reports the mean, standard deviation, and range of experimental failure load separately for stance and side configurations. Descriptive statistics of radiography, DXA, quantitative CT, and FEM variables are provided in Appendix E1 (online). The 80 femurs had a mean T score of −2.59 ± 0.89 (range, −0.99 to −4.38); 46 (58%) femurs were osteoporotic, including 20 femur pairs and six individual femurs.

Coefficients of determination (r^2) linking variables from each method to experimental failure load are reported in Appendix E1 (online), and selected graphs of linear regression are provided in Figure 5. In both configurations, 13 radiography parameters correlated significantly with failure load, with r^2 values ranging from 0.13 ($P = .024$) to 0.51 ($P < .001$) for stance and from 0.16 ($P = .014$) to 0.56 ($P < .001$) for side. In both configurations, the correlation was stronger with ITW. Nonsignificant correlations were found for neck shaft angle and for inferior and superior cortical femoral neck and shaft thicknesses.

The areal BMD value explained 65%–74% ($P < .001$) of failure load variance in the stance configuration

and 66%–80% ($P < .001$) of failure load variance in the side configuration. Correlations were strongest for areal BMD in the total hip and for areal BMD in the greater trochanter for stance and side configurations, respectively.

In the stance configuration, the quantitative CT variables explained 11%–72% of the failure load. The coefficient of determination was highest for the cross-sectional moment of inertia in the NeckBOX VOI (integral axial cross-sectional moment of inertia along the y-axis, $r^2 = 0.72$; $P < .001$). In the side configuration, all quantitative CT variables correlated significantly with failure load, and each variable alone explained more than 13% of the failure load variance. The most powerful variable was the integral BMC in the TrochanterSection, which alone explained 79% of the failure load variance ($P < .001$). In both configurations and for all VOIs, BMC variables correlated more strongly with the experimental failure load than did BMD variables. The numerical failure loads determined with FEM explained 87% and 83% of failure loads in stance and side configurations, respectively.

For radiography and quantitative CT modalities, because of the large number of variables (16 and 64, respectively), we first identified the most significant variables by using the random forest approach to avoid overfitting. The models that correlated best with the experimental failure load for each imaging modality are provided in Table 2. For quantitative CT, we computed two models by using either BMC or BMD parameters. In the stance and side configurations, respectively, the radiography models explained 66%

and 65% of the failure load; the DXA models, 73% and 80%; the quantitative CT models, 78% and 85%; and FEM, 87% and 83%. The radiography model for both configurations combined the ITW and a cortical thickness; this last parameter was the medial cortical femoral shaft thickness in the stance configuration and the lateral middiaphyseal thickness in the side configuration. The DXA model included one variable for each configuration, namely, areal BMD for the total hip in the stance configuration and areal BMD for the greater trochanter in the side configuration.

The quantitative CT models combined moments of inertia and a density variable, either BMC or BMD. The two models explained 78% of failure load in the stance configuration and 84%–85% of failure load in the side configuration. The AIC values suggested that estimation of the experimental failure load increased in accuracy from radiography to DXA and from DXA to quantitative CT, and that accuracy was greatest with FEM.

Models obtained after combining (a) all radiography and DXA parameters and (b) all quantitative CT and DXA parameters are reported in Table 3. In the stance configuration, strong failure prediction was enabled by a radiography and DXA model including ITW and areal BMD in the total hip ($r^2 = 0.82$). Similarly high prediction was yielded by using a DXA and quantitative CT model ($r^2 = 0.80$). In the side configuration, the model combining radiography and DXA variables explained 84% of the failure load. The model combining DXA and quantitative CT variables showed even better predictive performance ($r^2 = 0.86$).

Discussion

In our study, we assessed the performance of four methods in predicting the femoral failure load during mechanical testing in the stance and side configurations. The methods involved either simple radiography or DXA measurements or more sophisticated quantitative CT or FEM techniques. The results show that failure load is
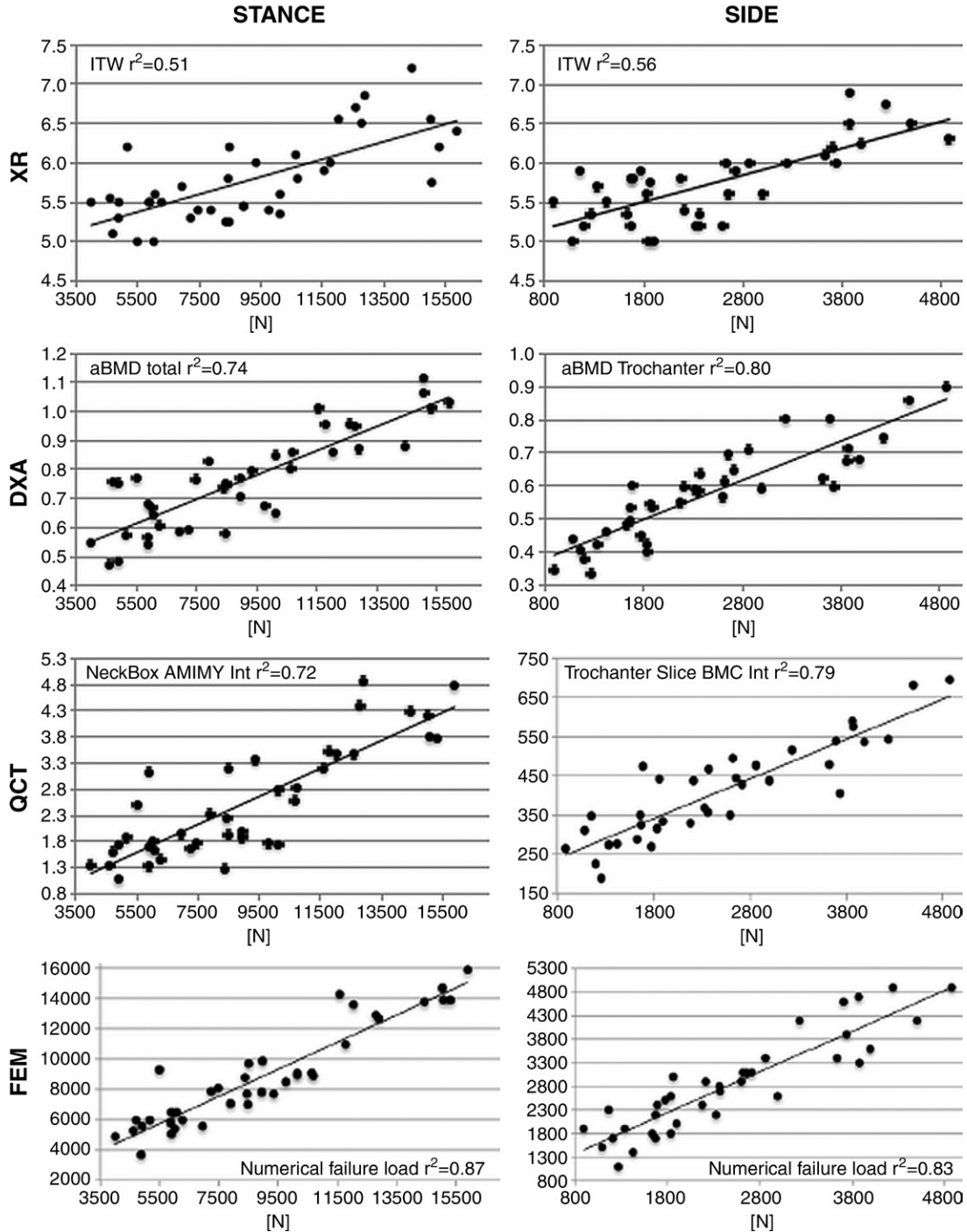
Figure 5

Figure 5: Linear regression graphs in the stance and side configurations for the three imaging-related methods and for FEM reporting the parameter most closely related to the mechanical failure load (in newtons). *aBMD* = areal BMD, *NeckBox AMIMY Int* = integral axial cross-sectional moment of inertia along the *y*-axis in the NecKBOX, *QCT* = quantitative CT, *Trochanter Slice BMC Int* = integral bone mineral content in the TrochanterSection, *XR* = radiography.

Imaging Techniques and Models Showing the Strongest Correlation with Experimental Failure Load

Modality and Variable	Coefficient	95% Confidence Interval	Adjusted r^2	AIC
		Stance		
Hip radiography				
ITW	4299	2989, 5609	0.66 ($P < .001$)	722
MCFS	2670	8238, 19070	…	…
DXA				
Total areal BMD	17587	15012, 20162	0.73 ($P < .001$)	714
Quantitative CT				
BMD				
NeckBox VOI AMIMY integral	21	13, 39	0.78 ($P < .001$)	710
Cortical mass weighted axial cross-sectional moment of inertia in the TrochanterSection	4279	96, 8462	…	…
NeckBox trabecular VOI BMD	941	−493, 2376	…	…
BMC				
Integral mass weighted axial cross-sectional moment of inertia in the TrochanterSection	3028	−351, 6407	0.78 ($P < .001$)	711
NeckBox VOI AMIMZ Int	1661	404, 3726	…	…
InterTrochanter VOI BMC Int	0.47	0, 2	…	…
FEM				
Numerical failure load	0.97	0.85, 1.08	0.87 ($P < .001$)	671
		Side		
Hip radiography				
ITW	1142	562, 1632	0.65 ($P < .001$)	574
LCMD	2991	1382, 4600	…	…
DXA				
Trochanter areal BMD	4280	19, 8541	0.80 ($P < .001$)	567
Quantitative CT				
BMD				
TrochanterSection cortical polar cross-sectional moment of inertia	−10158	−19742, −574	0.85 ($P < .001$)	561
Cortical mass weighted axial cross-sectional moment of inertia in the TrochanterSection	13214	1788, 24639	…	…
TrochanterVOI BMD Int	4.6	0, 8	…	…
BMC				
TrochanterSlice cortical polar moment of inertia	143	23, 264	0.84 ($P < .001$)	564
NeckBox AMIMZ Int	478	55, 900	…	…
TrochanterSection BMC Int	3.5	0, 6	…	…
FEM				
Numerical failure load	0.95b	0.8, 1.1	0.83 ($P < .001$)	559

Note.—The models (radiography, DXA, and quantitative CT) were performed with stepwise regression (backward selection) after identification of the most significant parameters by using the random forest procedure (overfitting detection). For each imaging technique, we computed the variables with their 95% confidence interval, coefficient, and coefficient of determination (adjusted r^2), as well as AIC. FEMs were performed with linear regression. AMIM = maxMA along the superoinferior neck axis; AMIMY or AMIMZ = axial cross-sectional moment of inertia along the y-axis or z-axis; Int = integral; LCMD = lateral cortical middiaphyseal thickness; MCFS = medial cortical femoral shaft thickness.

best predicted by using models based on both bone geometry and BMD or BMC. In both configurations, combining two geometric radiography parameters explained 65%–66% of the failure load variance. These two parameters were ITW and cortical thickness at the shaft (medially in the stance configuration, laterally in the side configuration).

The major contribution of cortical thickness to femoral strength has been shown in previous studies (8,22), including one based on radiographs obtained in vivo (8). In that study (8), two of the four radiography variables that best predicted fracture risk were cortical thicknesses, one at the neck and the other at the femoral shaft; the third variable was ITW. Similarly, in a retrospective case-control study, thinning of the medial shaft cortex measured on DXA images was associated with increased risk of hip fracture (22). The performance of radiography may be further improved by measuring an index of tensile trabeculae (8) or by computing textural parameters, such as entropy or homogeneity (16).

The areal BMD value obtained with DXA explained 73%–80% of the failure load variance. Furthermore, areal BMD in the total hip and that in the greater trochanter were particularly effective in the prediction of failure load in the stance and side configurations, respectively. Failure load was predicted less well in the stance configuration than in the side configuration. Our results are in agreement with those in several publications (23–25), some of which indicate a closer association of trochanteric fractures with low BMD than with cervical fractures, for which geometric parameters play a greater role. In our multivariate analyses, adding radiography variables to areal BMD in the total hip as measured with DXA increased the predictive performance from 73% to 80% in the stance configuration and from 82% to 84% in the side configuration. The addition of geometry to BMD increased the proportion of explained failure load variance, most notably in the stance configuration. Measurement of geometric parameters directly on

DXA images may yield different values compared with those obtained with radiography, as DXA has lower spatial resolution. Nevertheless, geometric parameters measured on DXA images contributed to in vivo hip fracture prediction independently from BMD (22,26).

Our models combining quantitative CT parameters explained 78%–85% of the failure load variance for both configurations. In both configurations, the best quantitative CT models combined a geometric parameter and a density parameter. The first point emphasized by our quantitative CT results is that in vitro, BMC is a better predictor of failure load than is BMD; this finding is in agreement with findings in a previous report (27). The second major point is the relevance of cross-sectional moments of inertia, which combine geometry with density distribution. At univariate analysis, the cross-sectional moment of inertia with respect to the superoinferior axis of the integral compartment of the NeckBOX VOI yielded the highest coefficient of determination in the stance configuration (r^2 = 0.72), and the cross-sectional moment of inertia with respect to the anteroposterior axis of the cortical compartment of

TrochanterSection yielded one of the highest coefficients of determination in the side configuration (r^2 = 0.77). The importance of moments of inertia was pointed out 30 years ago (28). The elastic properties of bone in torsion are closely related to these moments. A more recent study (29) showed that cross-sectional moments of inertia are strongly associated with bone strength as measured with FEM. In the side configuration, one of the most effective parameters was the cross-sectional moment of inertia in the cortex, a finding that further supports the major contribution of this compartment to femoral strength. Moreover, our study highlights the importance of the trochanteric region, with r values of 0.75 and 0.80 in the stance and side configurations, respectively (integral BMD in the TrochanterSection VOI for both). This quantitative CT result is consistent with our finding that ITW and areal BMD in the trochanteric region were effective radiography and DXA predictors, respectively. It is also consistent with two other studies in our group, one in vitro (30) and the other in vivo (10), in which femurs were analyzed by using the aforementioned three-dimensional dedicated femur

software, as well as with another in vivo study (31).

The numerical failure load value yielded by FEM explained 87% and 83% of failure load variance in the stance and side configurations, respectively (ie, higher proportions than with the other three methods, particularly for the stance configuration). These results are consistent with those of other studies (27,32–34). Quantitative CT-based FEM combining density and geometric parameters has been shown to be highly effective in fracture risk prediction (35,36). FEM processing times have been considerably shortened, even with standard desktop computers, and FEM models are now highly mature. These advances suggest that FEM may be able to gain widespread acceptance as a tool with which to predict femur fracture. Nevertheless, combining (a) radiography and DXA variables or (b) DXA and quantitative CT variables yielded coefficient of determination values similar to those obtained with FEM. These results raise questions about the additional contributions of FEM, which is a complex and costly technique, in assessment of the hip fracture risk in clinical practice (37). However, according to the AIC, FEM was more accurate in estimating the failure load than was quantitative CT, radiography, or DXA, whether alone or in combination; this point should be kept in mind when one develops treat-to-target strategies for osteoporotic hip fractures. We also need an in vivo evaluation of the performance of the four modalities. Feasibility and socioeconomic aspects would then deserve investigation should the results show a significant difference in performance.

Our study had several strengths. It provided evidence about the comparative efficacy of three imaging methods (radiography, DXA, and quantitative CT) and FEM in prediction of experimental failure load in the proximal femur. Furthermore, we evaluated failure loads in two configurations, stance and side, to simulate the conditions of cervical and trochanteric fractures, respectively. Finally, we studied 80 femurs, a larger number than in most previous

studies. A limitation of our study was the large number of quantitative CT variables. However, we used a rigorous statistical approach to avoid inflationary bias, and we checked our data for multicollinearity. Also, as reported previously (36,38), failure load prediction was less effective in the stance configuration than in the side configuration, a finding for which we had no explanation. Another limitation was the manual measurement of radiographic variables on film hard copies. This step was conducted before our imaging department was fully equipped with digital radiography. It may have adversely affected some of the radiographic measurements, particularly small dimensions, such as the cortical thickness of the femoral neck, thereby explaining the weak correlations of these measurements with failure load. It would have been interesting to interpret the results of each test configuration under the assumption that each produced the expected type of fracture (cervical for stance configuration, trochanteric for side configuration). However, the side configuration yields various fracture types, of which only 60% are trochanteric fractures (39) (not recorded in our study). Finally, the determinants of a fracture induced by mechanical testing cannot be extrapolated to in vivo situations, in which fractures are the consequence of many internal and external factors and of their complex interactions. Nevertheless, the main determinant of a hip fracture is the fall; a person with weak bones who does not fall will not experience a fracture.

In conclusion, quantitative CT-based FEM was the best method with which to predict the experimental failure load. However, by combining quantitative CT and DXA variables, we attained a performance as good as that attained with FEM. The combination of quantitative CT and DXA may be easier to use in fracture prediction, provided standardized software is developed. Our findings highlight the major influence on femoral strength, particularly in the trochanteric region, of a densitometric parameter combined with a geometric parameter.

References

1. Cummings SR, Melton LJ. Epidemiology and outcomes of osteoporotic fractures. Lancet 2002;359(9319):1761–1767.

2. Fox KM, Cummings SR, Williams E, Stone K; Study of Osteoporotic Fractures. Femoral neck and intertrochanteric fractures have different risk factors: a prospective study. Osteoporos Int 2000;11(12):1018–1023.

3. Cooper C, Campion G, Melton LJ 3rd. Hip fractures in the elderly: a world-wide projection. Osteoporos Int 1992;2(6):285–289.

4. Assessment of fracture risk and its application to screening for postmenopausal osteoporosis: report of a WHO study group. World Health Organ Tech Rep Ser 1994;843:1–129.

5. Trémollieres FA, Pouillès JM, Drewniak N, Laparra J, Ribot CA, Dargent-Molina P. Fracture risk prediction using BMD and clinical risk factors in early postmenopausal women: sensitivity of the WHO FRAX tool. J Bone Miner Res 2010;25(5):1002–1009.

6. Schuit SC, van der Klift M, Weel AE, et al. Fracture incidence and association with bone mineral density in elderly men and women: the Rotterdam study. Bone 2004;34(1):195–202.

7. Pulkkinen P, Partanen J, Jalovaara P, Jämsä T. Combination of bone mineral density and upper femur geometry improves the prediction of hip fracture. Osteoporos Int 2004;15(4):274–280.

8. Glüer CC, Cummings SR, Pressman A, et al. Prediction of hip fractures from pelvic radiographs: the study of osteoporotic fractures—the Study of Osteoporotic Fractures Research Group. J Bone Miner Res 1994;9(5):671–677.

9. Popp AW, Buffat H, Eberli U, et al. Microstructural parameters of bone evaluated using HR-pQCT correlate with the DXA-derived cortical index and the trabecular bone score in a cohort of randomly selected premenopausal women. PLoS One 2014;9(2):e88946. [Published correction appears in PLoS One 2014;9(5):e98167.]

10. Bousson V, Le Bras A, Roqueplan F, et al. Volumetric quantitative computed tomography of the proximal femur: relationships linking geometric and densitometric variables to bone strength—role for compact bone. Osteoporos Int 2006;17(6):855–864.

11. Danielson ME, Beck TJ, Karlamangla AS, et al. A comparison of DXA and CT based methods for estimating the strength of the femoral neck in post-menopausal women. Osteoporos Int 2013;24(4):1379–1388.

12. Cheng X, Li J, Lu Y, Keyak J, Lang T. Proximal femoral density and geometry measurements by quantitative computed tomography: association with hip fracture. Bone 2007;40(1):169–174.

13. Keyak JH, Sigurdsson S, Karlsdottir GS, et al. Effect of finite element model loading condition on fracture risk assessment in men and women: the AGES-Reykjavik study. Bone 2013;57(1):18–29.

14. Keaveny TM, Hoffmann PF, Singh M, Palermo L, Bilezikian JP, Greenspan SL et al. Femoral bone strength and its relation to cortical and trabecular changes after treatment with PTH, alendronate, and their combination as assessed by finite element analysis of quantitative CT scans. J Bone Miner Res 2008;23:1974–1982.

15. Kang Y, Engelke K, Kalender WA. A new accurate and precise 3-D segmentation method for skeletal structures in volumetric CT data. IEEE Trans Med Imaging 2003;22(5):586–598.

16. Chappard C, Bousson V, Bergot C, et al. Prediction of femoral fracture load: cross-sectional study of texture analysis and geometric measurements on plain radiographs versus bone mineral density. Radiology 2010;255(2):536–543.

17. Bergot C, Bousson V, Meunier A, Laval-Jeantet M, Laredo JD. Hip fracture risk and proximal femur geometry from DXA scans. Osteoporos Int 2002;13(7):542–550.

18. Duchemin L, Mitton D, Jolivet E, Bousson V, Laredo J, Skalli W. An anatomical subject-specific FE-model for hip fracture load prediction. Comput Methods Biomech Biomed Engin 2008;11(2):105–111.

19. Cody DD, Gross GJ, Hou FJ, Spencer HJ, Goldstein SA, Fyhrie DP. Femoral strength is better predicted by finite element models than QCT and DXA. J Biomech 1999;32(10):1013–1020.

20. Breiman L, Cutler A, Liaw A, Wiener M. randomForest Breiman and Cutler's Random Forest's for Classification and Regression, R Package version 4.5-30. https://www.stat.berkeley.edu/~breiman/RandomForests/

21. Akaike H. A new look at the statistical model identification. IEEE Trans Automat Contr 1974;19(6):716–723.

22. El-Kaissi S, Pasco JA, Henry MJ, et al. Femoral neck geometry and hip fracture risk: the Geelong osteoporosis study. Osteoporos Int 2005;16(10):1299–1303.

23. Duboeuf F, Hans D, Schott AM, et al. Different morphometric and densitometric parameters predict cervical and trochanteric hip fracture: the EPIDOS Study. J Bone Miner Res 1997;12(11):1895–1902.

24. Pulkkinen P, Partanen J, Jalovaara P, Jämsä T. BMD T-score discriminates trochanteric fractures from unfractured controls, whereas geometry discriminates cervical fracture cases from unfractured controls of similar BMD. Osteoporos Int 2010;21(7):1269–1276.

25. Gnudi S, Ripamonti C, Lisi L, Fini M, Giardino R, Giavaresi G. Proximal femur geometry to detect and distinguish femoral neck fractures from trochanteric fractures in postmenopausal women. Osteoporos Int 2002;13(1):69–73.

26. Faulkner KG, Cummings SR, Black D, Palermo L, Glüer CC, Genant HK. Simple measurement of femoral geometry predicts hip fracture: the study of osteoporotic fractures. J Bone Miner Res 1993;8(10):1211–1217.

27. Dall'Ara E, Luisier B, Schmidt R, Kainberger F, Zysset P, Pahr D. A nonlinear QCT-based finite element model validation study for the human femur tested in two configurations in vitro. Bone 2013;52(1):27–38.

28. Martens M, Van Audekercke R, De Meester P, Mulier JC. The geometrical properties of human femur and tibia and their importance for the mechanical behaviour of these bone structures. Arch Orthop Trauma Surg 1981;98(2):113–120.

29. Varghese B, Short D, Hangartner T. Development of quantitative computed-tomography-based strength indicators for the identification of low bone-strength individuals in a clinical environment. Bone 2012;50(1):357–363.

30. Yang L, Burton AC, Bradburn M, et al. Distribution of bone density in the proximal femur and its association with hip fracture risk in older men: the osteoporotic fractures in men (MrOS) study. J Bone Miner Res 2012;27(11):2314–2324.

31. Bousson VD, Adams J, Engelke K, et al. In vivo discrimination of hip fracture with quantitative computed tomography: results from the prospective European Femur Fracture Study (EFFECT). J Bone Miner Res 2011;26(4):881–893.

32. van den Munckhof S, Zadpoor AA. How accurately can we predict the fracture load of the proximal femur using finite element models? Clin Biomech (Bristol, Avon) 2014;29(4):373–380.

33. Engelke K, Libanati C, Fuerst T, Zysset P, Genant HK. Advanced CT based in vivo methods for the assessment of bone density, structure, and strength. Curr Osteoporos Rep 2013;11(3):246–255.

34. Link TM. Osteoporosis imaging: state of the art and advanced imaging. Radiology 2012;263(1):3–17.

35. Orwoll ES, Marshall LM, Nielson CM, et al. Finite element analysis of the proximal femur and hip fracture risk in older men. J Bone Miner Res 2009;24(3):475–483.

36. Keyak JH, Sigurdsson S, Karlsdottir G, et al. Male-female differences in the association between incident hip fracture and proximal femoral strength: a finite element analysis study. Bone 2011;48(6):1239–1245.

37. Zysset P, Qin L, Lang T, et al. Clinical use of quantitative computed tomography-based finite element analysis of the hip and spine in the management of osteoporosis in adults: the 2015 ISCD Official Positions—part II. J Clin Densitom 2015;18(3):359–392.

38. Koivumäki JE, Thevenot J, Pulkkinen P, et al. Cortical bone finite element models in the estimation of experimentally measured failure loads in the proximal femur. Bone 2012;51(4):737–740.

39. Cheng XG, Lowet G, Boonen S, et al. Assessment of the strength of proximal femur in vitro: relationship to femoral bone mineral density and femoral geometry. Bone 1997;20(3):213–218.